An Ultra-Compact 26/33 GHz Frequency-Reconfigurable Bi-Directional PA/LNA Front-End with >33/>24 dB Cross-Band Rejection

Haibin Yang, Tao Zhang, Xiaoxian Liu, Qijun Lu, Bowen Wang, Bei Liu, Lisheng Chen, Xin An, Shubin Liu, and Zhangming Zhu
Key Laboratory of Analog Integrated Circuits, Hangzhou Institute of Technology, and School of Integrated Circuit, Xidian University
Xi'an, China
Email: zhangt@xidian.edu.cn

***Abstract*—This paper presents an ultra-compact 26/33 GHz frequency-reconfigurable bi-directional power amplifier (PA) / low-noise amplifier (LNA) front-end for millimeter-wave applications. A novel bi-directional amplifier core with a built-in switchable LC-tank is proposed, which maintains the LNA device in the off-state even under large-signal conditions in PA mode, enhances gain while reducing the noise figure (NF) in LNA mode, and mitigates the impedance matching trade-off between PA optimum output 1-dB compression point (OP1dB) /power-added efficiency (PAE) and LNA optimum NF. Leveraging a high-Q parallel switchable inductor structure, a frequency-reconfigurable and notch-adjustable interstage matching network is designed. In LNA mode, the prototype achieves measured 18.5/16.6 dB peak gain, 5.2-5.9/5.5-6.3 dB NF in low-/high-frequency band, respectively. In PA mode, it achieves 16/17 dB peak gain, 18.5%/15.2% peak PAE, and 13.5/13.3 dBm OP1dB in low-/high-frequency bands, respectively. Additionally, it features >33/>24 dB cross-band rejection across high-/low-frequency band, respectively.**

Keywords—bi-directional, frequency-reconfigurable, ultra-compact, PA/LNA, millimeter-wave, cross-band rejection

I. Introduction

Exponentially growing wireless data demands necessitate the use of multiple millimeter-wave (mm-wave) frequencies, which offer abundant available bandwidth. However, the severe free-space path loss and limited performance of silicon-based RF ICs at such high frequencies must be overcome, necessitating the deployment of large-scale phased array transceivers. Concerning the considerable number of front-ends (FEs), area-efficient multi-band FEs are essential for achieving low-cost and compact designs.

As shown in Fig. 1, compared to conventional transceiver (TRX) architectures, which consist of a power amplifier (PA) and a low-noise amplifier (LNA) placed in parallel with a T/R switch for mode control, bi-directional FEs are gaining popularity due to their potential to minimize FE area and cost. Several bi-directional PA/LNA structures [1]-[6] have been presented, but they typically operate in a single narrow band. To support multiple mm-wave bands, one solution involves implementing ultra-broadband FEs. However, this approach suffers from limited RF performance and cross-band interference. Alternatively, frequency-reconfigurable (FR) FEs offer a better balance between area and cross-band rejection (CBR). In [7]-[9], FR techniques using switched capacitors and inductors are presented to meet multi-band requirements. However, when directly applied to conventional bi-directional FEs, these techniques require additional switches to toggle between TX and RX modes, leading to significant losses in the FR matching network

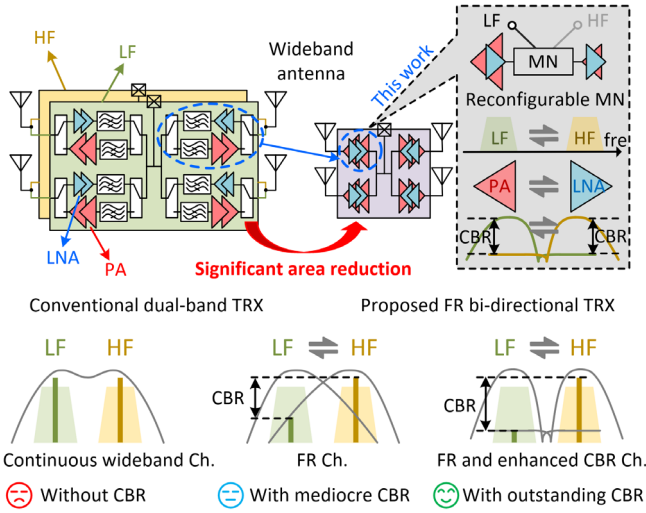

Fig. 1. Comparison of block diagrams and concepts of different TRX topologies for multi-band applications.

(MN). Therefore, these FR FEs are typically unidirectional and lack effective CBR.

To address these issues, this paper presents an ultra-compact FR bi-directional PA/LNA FE with enhanced CBR for the first time. A novel bi-directional amplifier core with a built-in switchable LC-tank is proposed to improve both PA/LNA mode performances and mitigate the impedance matching trade-off between PA optimum output 1-dB compression point (OP1dB) / power-added efficiency (PAE) and LNA optimum noise figure (NF). Instead of a conventional lossy coupled switchable inductor [9], a high-Q parallel switchable inductor is used to implement the FR MN, ensuring minimal performance degradation during frequency reconfiguration. Additionally, a shared FR MN incorporating a notch-adjustable filter is implemented, achieving > 33 dB/> 24 dB CBR across the high-/low-frequency bands,.

II. Bi-directional Core With Built-in Switchable LC-Tank

Fig. 2 illustrates the proposed bi-directional PA/LNA core topology compared with the conventional bi-directional core topologies. The bi-directional core presented in [1] employs a differential neutralized common-source stage controlled by tail switches [see Fig. 2 (a)]. However, in PA mode, the limitations in device drain/gate biasing (ensuring $V_{D\text{-}PA}$-$V_{G\text{-}PA}$<$V_{th\text{-}LNA}$) and the undesired turn-on of the off-state LNA devices degrade the PA output power, linearity, and efficiency. To address these issues, the bi-directional core in [2] utilizes a hybrid N/PMOS PA/LNA topology to enhance PA performance [see Fig. 2 (b)]. Nevertheless, this design compromises the NF and power gain in LNA mode.

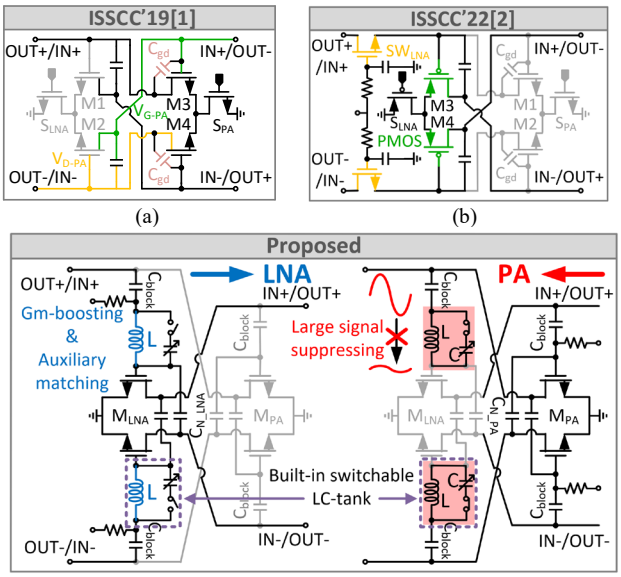

Fig. 2. (a) Conventional neutralized bi-directional PA/LNA core. (b) Conventional Hybrid N/PMOS bi-directional PA/LNA core. (c) The proposed PA/LNA core with a built-in switchable LC-tank.

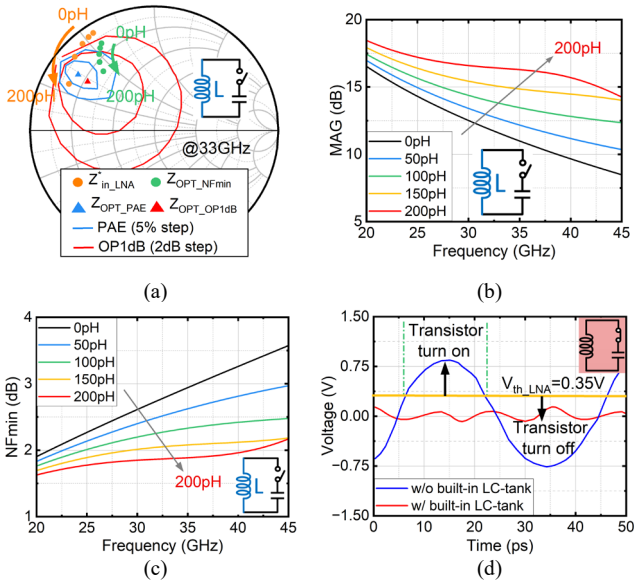

Fig. 3. Comparison of (a) impedance (b) LNA MAG (c) LNA NFmin and (d) voltage swing at the gate of LNA in PA mode with and without the built-in switchable LC-tank.

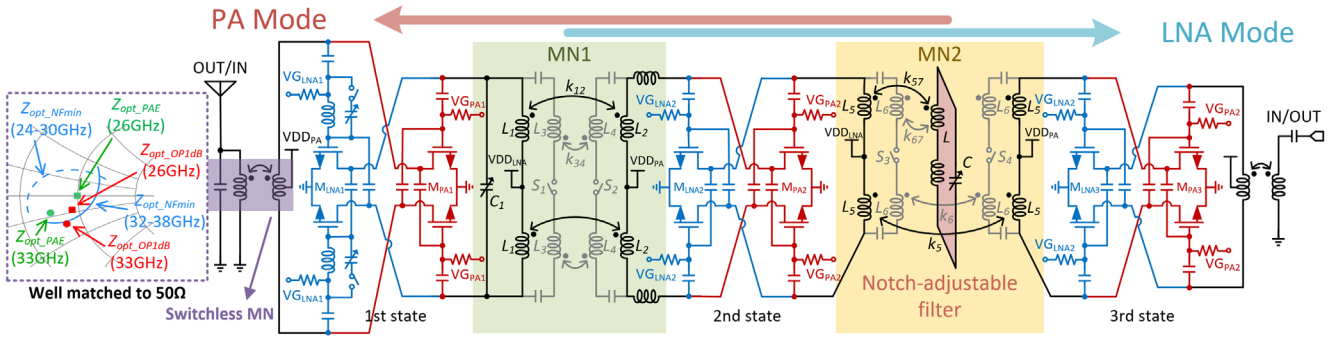

Fig. 4. Schematic of the proposed bi-directional PA/LNA and EM simulated result of the input MN.

In this work, a novel bi-directional PA/LNA core with a built-in switchable LC-tank is proposed. In LNA mode, the switchable LC-tank functions as a g_m-boosting inductor, effectively minimizing the differences among the optimum impedances ($Z_{opt\text{-}OP1dB}$, $Z_{opt\text{-}PAE}$, $Z^*_{in\text{-}LNA}$, and $Z_{opt\text{-}NFmin}$) of the PA and LNA [see Fig. 3 (a)], increasing the maximum available gain (MAG) [see Fig. 3 (b)], and, reducing the NF_{min} [see Fig. 3 (c)]. In PA mode, the switchable LC-tank acts as a high-impedance parallel LC resonator, keeping the LNA device in the off-state even under large-signal conditions [see Fig. 3 (d)], thereby improving PA output power and efficiency. Due to the mismatch between the gate-drain capacitance (C_{gd}) of the off- (M1/M2) and on-state (M3/M4) transistors, the C_{gd} of M3/M4 (see Fig. 2) cannot fully neutralized in [1] and [2]. As a result, the bi-directional PA/LNA cores may not maintain unconditional stability. To address this issues, separate passive capacitors ($C_{N\text{-}PA}$ and $C_{N\text{-}LNA}$) are employed to achieve individual optimal neutralization in PA and LNA modes. DC block capacitors C_{block} are also introduced to separate the PA and LNA bias voltages, enabling each to operate at its optimal bias point.

III. Circuit Implementation

Fig. 4 illustrates the schematic of the proposed FR bi-directional PA/LNA. It consists of a proposed bi-directional PA/LNA core and two bi-directional driving cores, with the passive components shared in the PA and LNA modes. Notably, the input/output MNs are switchless, while the interstage MNs are FR. As mentioned above, benefiting from the g_m-boosting inductor of the built-in switchable LC-tank, the impedance matching trade-off between PA optimum OP1dB/PAE and LNA optimum NF is efficiently alleviated, simplifing to realize low-loss and wideband MN. In Fig. 4, the $Z_{opt\text{-}OP1dB}$, $Z_{opt\text{-}PAE}$, and $Z_{opt\text{-}NFmin}$ of PA/LNA are all well-matched to 50 Ω (antenna) across both the low-frequency (LF) and high-frequency (HF) bands with the switchless MN.

A. High-Q Parallel Switchable Inductor for FR XFMR

For FR MN design, embedding a switched capacitor degrades circuit performance, leading to increased insertion loss at lower frequencies, reduced relative bandwidth, and higher parasitic losses [8]. Alternatively, switched-inductor MNs using coupled switchable inductors have been proposed [9]. However, the coupled switchable inductor suffers from a low Q factor, resulting in higher matching loss during frequency reconfiguration. To address these issues, this work proposes an inductor-variable transformer-based FR MN that leverages a high-Q parallel switchable inductor to achieve a wide impedance tuning range and minimize losses.

Fig. 5 compares the performance of the conventional coupled switchable inductor and the parallel switchable inductor. As observed, the parallel switchable inductor maintains a higher Q factor across different inductor transformation ratios (L_{on}/L_{off}) and across the entire frequency band when L_{on}/L_{off} = 0.7. This improvement is attributed to the in-phase magnetic fields of the two coils in the parallel inductor, which enhance the total stored magnetic energy, thereby increasing the Q factor.

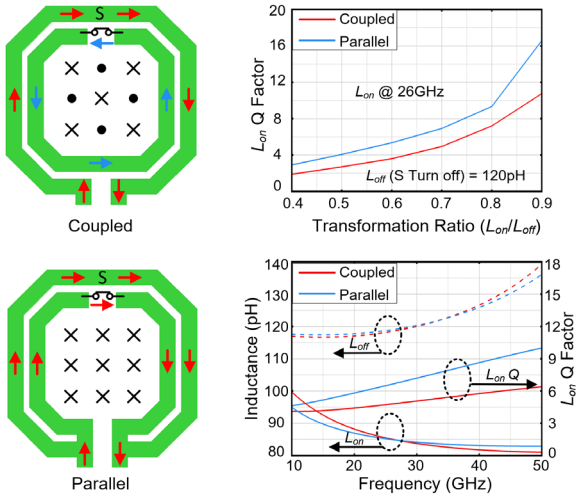

Fig. 5. Performance comparison with the conventional coupled switchable inductor and the proposed parallel switchable inductor.

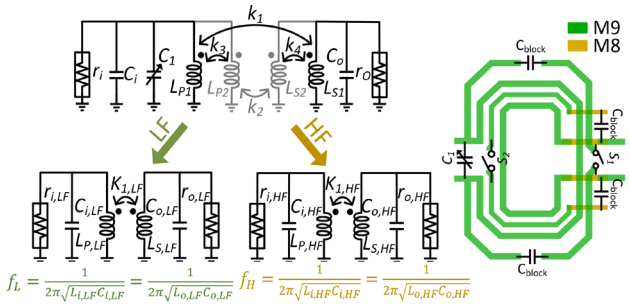

Fig. 6. (a) Equivalent circuit models, and (b) layout implementation.

B. *Frequency-Reconfigurable Matching Network Design*

The proposed inductor-variable transformer-based FR MN, utilizing a high-Q parallel switchable inductor, is implemented for the interstage MNs. Fig. 6 presents the circuit model of the interstage FR MN (MN1) between the first and second stages along with its layout implementation. Notably, the resonant frequency of the MCR (f_L/f_H) is determined by the parallel capacitors ($C_{i,LF}$, $C_{o,LF}/C_{i,HF}$, $C_{o,HF}$) and inductors ($L_{P,LF}$, $L_{S,LF}/L_{P,HF}$, $L_{S,HF}$). Therefore, by adjusting the inductance via the switches S_1 and S_2, the operating band can be effectively shifted. Noted that the switchable capacitor (C_1) is used to switch the MN for PA/LNA mode, accommodating the different input/output impedances of the first stage in PA and LNA modes.

To improve the CBR, the interstage FR MN (MN2) between the second and third stages is designed as a notch-adjustable 3rd-order filter by incorporating an additional LC resonator. Fig. 7 (a) and (b) present its circuit model and layout implementation. The FR MN with a notch-adjustable filter, based on a three-coil transformer, can be equivalently transformed into a series-shunt LC notch filter [10]. Noted that the resonant frequency of the notch filter is exclusively determined by the capacitor (C) and inductor (L). Therefore, by tuning the capacitor (C), the notch frequency can be effectively adjusted. Fig. 7 (c) shows the simulated S_{21} of the FR MN with and without the notch-adjustable filter, demonstrating an increase in notch depth of about 15 dB across the HF band and 10 dB across the LF band. Additionally, since the second and third stages share the same transistor size, MN2 is designed symmetrically, unlike interstage MN1, eliminating the need for additional configuration to toggle between PA and LNA modes. This approach removes the necessity for extra switches, reducing losses and simplifying the MN2 design.

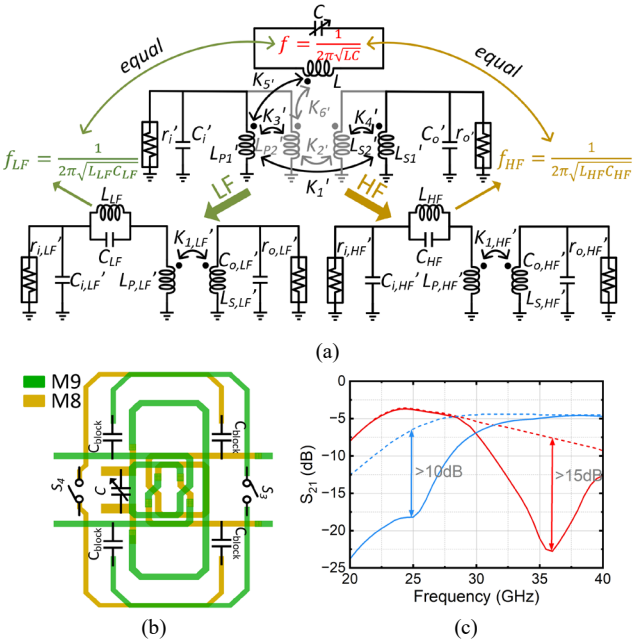

Fig. 7. (a) Equivalent circuit models, (b) layout implementation, and (c) EM simulated results of FR MN with/without notch filter.

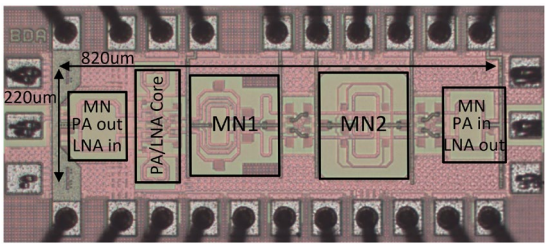

Fig. 8. Die micrograph of proposed FR PA/LNA.

IV. Measurement Result

The proposed FR bi-directional PA/LNA FE was implemented in a 65-nm CMOS process, and its chip micro-photograph is shown in Fig. 8. The core size, excluding the pads, is 820 × 220 μm^2. The dc power consumptions in PA and LNA modes are 141 mW and 76 mW, respectively.

Fig. 9 shows the simulated and measured results of S-parameters, NF, and IP1dB in LNA mode. In the LF band, the peak gain (S_{21}) is 18.5 dB at 26 GHz with a 3-dB bandwidth from 23.3 to 27.8 GHz, and the CBR is > 33 dB across the HF band. The minimum NF is 5.2 dB at 26 GHz, and the overall NF and IP1dB are < 5.9 dB and > -14 dBm in 3-dB bandwidth. In the HF band, the peak gain (S_{21}) is 16.6 dB at 34 GHz with a 3-dB bandwidth from 30.8 to 38.5 GHz, and the CBR is > 24 dB across the LF band. The minimum NF is 5.5 dB at 34 GHz, and the overall NF and IP1dB are < 6.3 dB and > -8dBm in 3-dB bandwidth.

Fig. 10 shows the simulated and measured results of S-parameters, OP1dB, Psat and PAE in PA mode. In the LF band, the peak gain (S_{21}) is 16 dB at 26 GHz with a 3-dB bandwidth from 23.7 to 28.3 GHz, and the CBR is > 34 dB across the HF band. Measurements show that the bi-directional FE achieves 18.5% peak PAE, 13.5 dBm OP1dB, and 14.8 dBm Psat, respectively. In the HF band, the peak gain (S_{21}) is 17 dB at 34 GHz with a 3-dB bandwidth from 30.7 to 36.6 GHz, and the CBR is > 27 dB across the LF

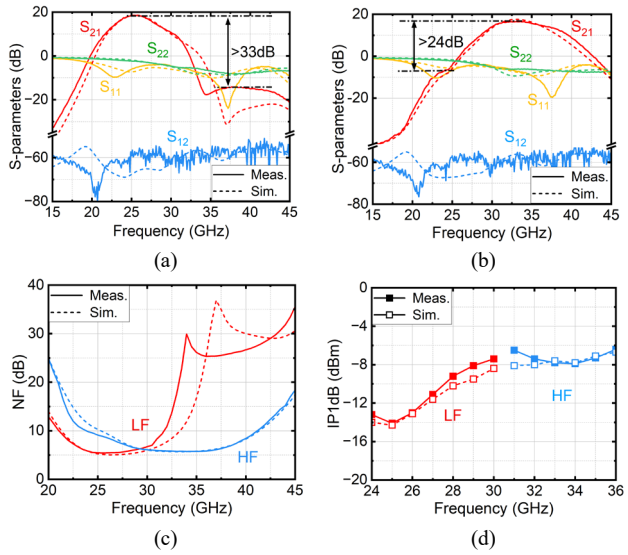

Fig. 9. Simulated and measured results of (a) LF mode S-parameters, (b) HF mode S-parameters, (c) NF, and (d) IP1dB in LNA mode.

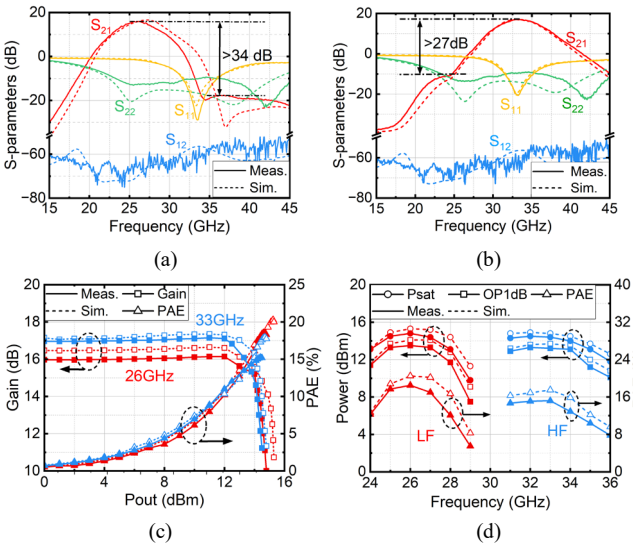

Fig. 10. Simulated and measured results of (a) LF mode S-parameters, (b) HF mode S-parameters, (c) gain and PAE at 26/33 GHz and (d) output power and PAE in hole band in PA mode.

band. Measurements show that the bi-directional FE achieves 15.2% peak PAE, 13.3 dBm OP1dB, and 14.5 dBm Psat.

Table I summarizes the performance of this work and its comparison with state-of-the-art PA/LNA FEs designs for mm-wave applications. Compared to existing solutions, the proposed PA/LNA FE supports both bi-directional operation and FR capability. Additionally, benefiting from the FR MN with a notch-adjustable filter, the PA/LNA FE achieves >33 dB/>24 dB CBR across the high-/low-frequency bands while maintaining competitive PA/LNA performance.

V. Conclusion

A FR bi-directional PA/LNA FE is presented in 65nm CMOS. Utilizing a novel bi-directional core with a built-in switchable LC-tank and low-loss FR MN with a notch-adjustable filter, the proposed FE achieves competitive PA/LNA performance with FR capability and >33/>24 dB CBR across the HF/LF bands. With these distinctive features, this design is expected to be one of the promising candidates for future multi-band 5G mm-wave applications.

TABLE. I. Comparison With State-of-the-Art PA/LNA FEs

		TMTT 25[3]	CICC 23[4]	VLSI 22[5]	JSSC 20[6]	TMTT 25[7]	This work
Technology		28 nm CMOS	40 nm CMOS	65 nm CMOS	65 nm CMOS	28 nm CMOS-SOI	**65 nm CMOS**
Topology		Bidir.	Bidir.	Bidir.	Bidir.	FR (Unidir.)	**Bidir.+FR**
PA	3-dB BW (GHz)	27.3~35.4	52.0~67.0	38.0~42.0#	26.5~29.5#	26.0~28.0 34.0~39.0	**23.7~28.3** **30.7~36.6**
PA	Gain(dB)	20.4	8.0	12.0*	12.0	18.5/18.4	**16.0/17.0**
PA	OP1dB(dBm)	15.0	12.8	16.0*	13.0	13.5/13.5	**13.5/13.3**
PA	Psat(dBm)	17.4	15.2	18.9	15.4	15.5/15.5*	**14.8/14.5**
PA	PAE(%)	17.2	9.3	30.4	20.0	15.5/14.1	**18.5/15.2**
PA	Pdc(mW)	N.A.	291	246	149	164/173	**141**
LNA	3-dB BW (GHz)	28.0~36.0	52.0~66.0	38.0~42.0#	26.5~29.5#	23.5~27.0 33.5~37.5	**23.3~27.8** **30.8~38.5**
LNA	Gain(dB)	17.3	11.3	N.A.	18.0*	16.4/19.1	**18.5/16.6**
LNA	NF(dB)	5.3~7.3*	6.8**	4.8(min)	4.6(28GHz)	4.4(min) 4.9(min)	**5.2~5.9** **5.5~6.3**
LNA	Pdc(mW)	63	78	56	31	63/54	**76**
CBR(dB)		NO	NO	NO	NO	>10/>6	**>33/>24**
Core area (mm^2)		0.10	0.08	0.26	0.11	0.48*	**0.18**
Supply(V)		3.0(PA) 1.0(LNA)	N.A.	1.0	N.A.	2.2(PA) 1.1(LNA)	**1.2(PA)** **1.0(LNA)**

*Estimated from the measured results
#TX/RX Operating bandwidth
Bidir.: Bi-directional
**Simulated Results
N.A.: Not available
Unidir.:Unidirectional

Acknowledgment

This work was supported by National Nature Science Foundation of China (No. 62374125, 62131013, 62021004, 62090040), and the Fundamental Research Funds for the Central Universities (No. JB191113).

References

[1] J. Pang *et al.*, "21.1 A 28GHz CMOS Phased-Array Beamformer Utilizing Neutralized Bi-Directional Technique Supporting Dual-Polarized MIMO for 5G NR," in *IEEE Int. Solid-State Circuits Conf.* (*ISSCC*), pp. 344–346, Feb. 2019.

[2] J. Park *et al.* "A 26-to-39GHz Broadband Ultra-Compact High-Linearity Switchless Hybrid N/PMOS Bi-Directional PA/LNA Front-End for Multi-Band 5G Large-Scaled MIMO System," in *IEEE Int. Solid-State Circuits Conf.* (*ISSCC*), pp. 322–324, Feb. 2022.

[3] J. Pang et al., "A 28-GHz CMOS Phased-Array Beamformer Utilizing Neutralized Bi-Directional Technique Supporting Dual-Polarized MIMO for 5G NR," *IEEE J. Solid-State Circuits*, vol. 55, no. 9, pp. 2371–2386, Sept. 2020.

[4] J. Hwang *et al.* "Compact Bi-Directional PA-LNA Using Stacked Power Amplifier Enhancing Linearity and Stability," *IEEE Trans. Microw. Theory Techn*, vol. 73, no. 4, pp. 2000-2008, April. 2025.

[5] H. Jia, Y. Wang and A. Zhu, "A 52-67GHz Ultra-Compact Bi-directional Gate-switching Cascode Amplifier with Tri-coil Broadband Matching in 40-nm CMOS," in *IEEE Custom Integrated Circuits Conference* (*CICC*), pp. 1-2, May. 2023.

[6] Z. Li *et al.*, "A 39-GHz CMOS Bi-Directional Doherty Phased-Array Beamformer Using Shared-LUT DPD with Inter-Element Mismatch Compensation Technique for 5G Base-Station," in *Proc. Symp. VLSI Circuits*, pp. 98-99, July. 2022.

[7] J. Lee *et al.*, "A 28/37-GHz Frequency-Reconfigurable Dual-Band 1-Channel Front-End IC for 5G Communication Radios, " *IEEE Trans. Microw. Theory Techn*, vol. 73, no. 4, pp. 1882-1895, April. 2025.

[8] F. Zhao, W. Deng, H. Jia, W. Ye, R. Wan, B. Chi, "A Band-Shifting Millimeter-Wave T/R Front-End Using Inductance-Mutation Transformer Technique for Multiband Phased-Array Transceivers, " *IEEE J. Solid-State Circuits*, vol. 59, no. 5, pp. 1323-1336, May. 2024.

[9] R. A. Shaheen *et al.* "Millimeter-wave Frequency Reconfigurable Low Noise Amplifiers for 5G, " IEEE Trans. on Circ. and Systems II: Express Briefs, vol. 68, no. 2, pp. 642-646, Feb. 2021.

[10] J. Zhang, D. Zhao, X. You, "Analysis and Design of a CMOS LNA With Transformer-Based Integrated Notch Filter for Ku-Band Satellite Communications, " *IEEE Trans. Microw. Theory Techn*, vol.70, no.1, pp. 790-800, Jan. 2022.